ELSEVIER

www.elsevier.nl/locate/jelechem

Journal of Electroanalytical Chemistry 491 (2000) 139–147

Journal of Electroanalytical Chemistry

Mercury–mercury tunneling junctions Part II. Structure and stability of symmetric alkanethiolate bilayers and their effect on the rate of electron tunneling

Krzysztof Slowinski, Marcin Majda *

Department of Chemistry, University of California at Berkeley, Berkeley, CA 94720-1460, USA

Received 13 April 2000; received in revised form 31 May 2000; accepted 13 July 2000

Dedicated to Professor E. Gileadi on the occasion of his retirement from the University of Tel Aviv and in recognition of his contribution to electrochemistry

Abstract

We have investigated electrical properties of symmetric alkanethiolate bilayer junctions formed by contacting two hanging mercury drop electrodes each coated initially with a single alkanethiolate monolayer. Using potentiodynamic, current transient and ac impedance methods, we have shown that the initial, largely all-*trans* structure of the bilayers becomes disordered with time as a result of the van der Waals and coulombic forces squeezing the junction. Chain disorder involves both *gauche* defects and chain intercalation at the mid plane of the bilayer. We showed that the latter progress more rapidly for junctions formed with longer alkanethiols. To characterize the strength of the electronic coupling across these junctions, we measured the decay constant β for the native bilayers featuring largely all-*trans* conformation and for the disordered junctions. The former was obtained from fast scan (50–500 V s^{-1}) j–V experiments and yielded $\beta = 1.29$ per CH_2 group (corresponding to $\beta = 1.0$ $Å^{-1}$). Impedance measurements were used to investigate properties of the disordered junctions. Electron tunneling resistance and junction capacitance were measured simultaneously. The plot of the logarithm of junction resistance measured at zero voltage bias versus thickness gave $\beta = 1.6$ $Å^{-1}$. These measurements demonstrate that the efficiency of electron tunneling decreases substantially when alkanethiolate chains become disordered.

Keywords: Tunneling junctions; Self assembled alkenthiolate bilayers; Electron tunneling

1. Introduction

Electron tunneling plays a critical role in many biological processes [1–5]. Electron tunneling is also of fundamental importance in a rapidly growing area of molecular electronics [6–8]. Consequently, the kinetics of long-range electron transfer (ET) across molecular fragments of specific chemical structure has been a topic of substantial interest [9–14]. An extensive body of experimental data collected in the investigations of both enzymatic [2–5] and synthetic systems [9,11,12,15] indicates that ET rates are sensitive not only to the distance but also to the structural details of a molecular fragment separating the electron donor and acceptor. In general, the electronic coupling matrix element decays exponentially with distance (d) according to Ref. [16]:

$$H_{DA}^2(d) = H_{DA}^2(d = 0) \exp(-\beta d)$$

where the magnitude of a decay constant, β, reflects the strength of the electronic coupling across a particular molecular bridge. Decay constants have been determined for various molecular systems. For example, tunneling efficiency through σ-bonded molecular fragments ($\beta = 0.78$–0.97 $Å^{-1}$) [14,17–19] is lower than through π-conjugated fragments ($\beta = 0.3$–0.1 $Å^{-1}$) [11,20,21], but more efficient than through a van der Waals bridge ($\beta = 1.3$ $Å^{-1}$) [14]. Recent experiments indicate that the presence of amide groups within a monolayer of hydrocarbon chains increases ET efficiency due, probably, to a network of lateral hydrogen

* Corresponding author.
E-mail address: majda@socrates.berkeley.edu (M. Majda).

0022-0728/00/$ - see front matter
PII: S0022-0728(00)00305-3

bonds [22,23]. On the other hand, Miller et al. have shown that the presence of a single triple or double bond or an ether group in a hydrocarbon chain slows down ET [12]. Analogous effects of protein structure on the electronic coupling strength were observed in electron transfer proteins [5,24]. Equally important, although more difficult to study, are conformational effects on the kinetics of ET. Theoretical calculations suggest that ET through disordered hydrocarbon chains is less efficient than ET through chains in all-*trans* conformation [25,26]. In an elegant experiment, Haran and co-workers have shown a decrease of the electron tunneling rate across a monolayer of octadecyltrichlorosilane (OTS) formed on a highly doped Si wafer when the initially all-*trans* structure of the monolayer was thermally disordered to induced *gauche* defects [27]. Surprisingly, the opposite effect was reported for a similar system by Boulas and co-workers [28].

A number of experimental approaches has been developed to study ET through well-defined synthetic molecular fragments. They involve photoinduced electron transfer between donor/acceptor pairs separated by a rigid bridging fragment [1,3,5,9], electrochemical methods [10,17,29], and a tunneling junction method [30,31]. In the latter case, two metal plates are separated by a thin organic film of known structure and thickness. Kuhn and co-workers investigated ET through long-chain fatty acids adsorbed on aluminum electrodes [32]. The second electrode was either a vapor-deposited metal (Me = Al or Pb) or mercury. They determined that conductance in these systems depends exponentially on monolayer thickness. A number of reports concerning Me-monolayer(multilayer)–Me type systems have been published since then [33–37]. Since in such experiments evaporation of the second metal is typically used in order to form a junction, existence of defects in the organic layer is a frequently encountered experimental problem of this approach leading to short circuits. More recently, other junction systems have been developed to measure rates of electron tunneling. These include 'break junctions' [38], nanofabricated electrodes [39], crossed wires [40] as well as the AFM (conducting mode) [41,42] and STM methods [43].

Mercury as a liquid metal offers atomically smooth, defect-free surfaces. These advantages make it a particularly suitable metal for assembly of tunneling junctions. Surprisingly, only a few reports have dealt so far with Hg–Hg type junctions. In addition to the work of Kuhn mentioned above [32], Porter and Zinn studied electron tunneling through ordered water layers trapped between two Hg drops [44]. The tunneling data were collected with an impedance technique immediately prior to the coalescence of the two drops that were slowly brought together in an aqueous electrolyte. To prevent coalescence of two mercury surfaces, the drops can be charged in an aqueous electrolyte, as demonstrated by Usui and co-workers [45]. A different method was reported by Rampi et al. who demonstrated that formation of alkanethiolate monolayers on mercury surfaces also prevents their coalescence [46]. While these authors did not measure tunneling currents, their capacitance measurements showed that the thickness of the films trapped in the Hg–Hg junctions was proportional to the length of the alkanethiols used in these experiments with $\varepsilon = 2.7$ indicating that the junctions consisted of alkanethiolate bilayers.

Our recent report demonstrated that tunneling currents can be measured reproducibly in the Hg–Hg type junctions when two small mercury drops, each coated with an alkanethiolate monolayer, are brought into contact [23]. These types of junctions are used in this report to investigate the effect of the structure of the alkanethiolate bilayers on the electron tunneling rates. Specifically, we used potentiodynamic and impedance techniques to follow the time evolution of the structure of the alkanethiolate bilayer in a junction. We discovered that a slowly progressing process of junction collapse, which depends on time, voltage bias and other factors, induces disorder of the initial all-*trans* structure of the bilayer before subsequent, progressive intercalation of the alkane chains of the two monolayers leads ultimately to the sudden collapse of a junction and coalescence of the Hg drops. We observed that as these events unfold the strength of the electronic coupling decreases during the initial, disorder stage of the junction collapse process. Thus we were able to measure two values of the decay constant: one representing the initially well-ordered alkane chains ($\beta = 1.0$ Å^{-1}) and the other corresponding to a disordered state of the alkane chains with $\beta = 1.6$ Å^{-1}.

2. Experimental

2.1. Reagents

Fresh samples of alkanethiols, C_nSH, $n = 9$, 10, 12, 14 and 16 were purchased from TCI America (95 + %) or from Aldrich. Hexadecane (Aldrich, 99 + %), mercury (Quicksilver Inc., triply distilled) and the alkanethiols were used as received.

2.2. Hg–Hg tunneling junctions

The mercury junctions were assembled using two locally constructed [23], micrometrically driven Kemula–Kublik type [47] hanging mercury drop electrodes (HMDE). The glass capillaries of the HMDEs were 250 μm in diameter and were silanized with OTS. The two electrodes were mounted vertically and coaxially, one above the other in a custom made aluminum stand. The tips of the capillaries could be aligned and the size of

the junctions measured with a long focal length microscope (Titan, Tool Supply Co. Inc.) affording a 100-fold magnification and equipped with a filar eye piece. The microscope was mounted on a semicircular rotating stage that allowed us to observe the two capillaries and the Hg drops at two angles 90° apart. To properly align the capillaries, the top electrode was attached to an $x–y–z$ micrometer stage (model M-460A, Newport Corp.). A small rectangular glass cell was mounted around and coaxially with the glass capillary of the bottom HMDE near its tip allowing for immersion of the tips of both capillaries in a desired alkanethiol solution or a pure solvent. Most experiments were done in 5–20% (v/v) hexadecane solutions of a selected alkanethiol. Thus the self-assembly of the alkanethiol monolayers took place momentarily upon generation of the new Hg drops. To assemble a junction, the Hg drops were generated with the two electrodes, they were aligned and then brought into contact as described in Section 3. The initial size of the Hg drops ranged from 0.025 to 0.045 cm^2. The former corresponds to the drop diameter of 0.089 cm. A typical junction diameter, which could be measured optically with ca. $\pm$ 5% precision, ranged from 0.015 to 0.046 cm. Within this experimental precision of our microscopic measurements, the junction diameter depended neither on voltage bias nor on the time elapsed since junction assembly.

2.3. Tunneling current and ac impedance measurements

All the measurements and data analyses were done with a CHI model 660A electrochemical analyzer/workstation (CH Instruments, Inc. Austin, TX).

3. Results and discussion

3.1. Assembly of $Hg–C_n–C_n–Hg$ junctions and their general characterization

The process of Hg–Hg junction formation consists of two steps. In the first step, the two mercury drops are generated independently and aligned in a junction cell filled with a hexadecane solution of a desired alkanethiol (see Fig. 1A). Subsequently, using the $x–y–x$ micrometer controlling the position of the top HMDE, the drops are brought into contact resulting in a small deliberately induced distortion of their shape as shown in Fig. 1B. While the drops are at open circuit in a hexadecane solution, microscopic observations of the drops at this stage suggest that their distortion is similar to that reported for two negatively charged (thus experiencing a repulsive potential) Hg drops in an aqueous electrolyte solution [45]. The second step of junction formation takes place spontaneously some 0.5–3 s later. At that point, a sudden 'twitch' of the drops is observed resulting in an enlargement of the apparent contact area as shown in Fig. 1C. When the same sequence of steps is carried out in an aqueous thiol solution (limited due to solubility to $C_9SH–C_{12}SH$), the final junction area is $\sim$ 50% larger. These observations lead us to conclude that the initial repulsion and the resulting drop distortion are due to a layer of solvent trapped between the two drops. Subsequently, the solvent is squeezed out, a process observed as a twitch of the drops, and the van der Waals attraction between two alkanethiolate monolayers on

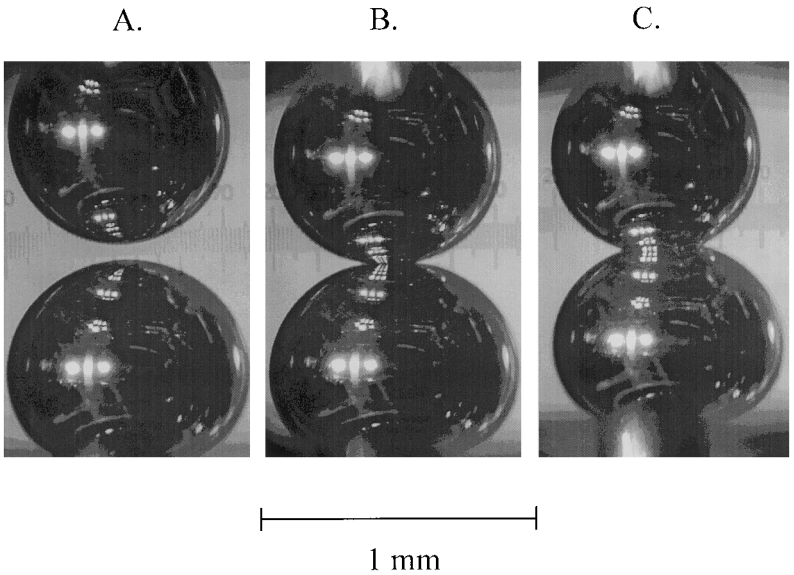

Fig. 1. Photographs illustrating the process of junction assembly. The two Hg drops are immersed in a 20% (v/v) solution of decanethiol in hexadecane. (A) Before junction formation. (B) Immediately after the drops are brought into contact. (C) After a 'twitch' of the drops resulted in complete solvent removal from the junction. Note that this process results in an increase of the junction area reflecting the existence of van der Waals attraction between the two decanethiolate monolayers.

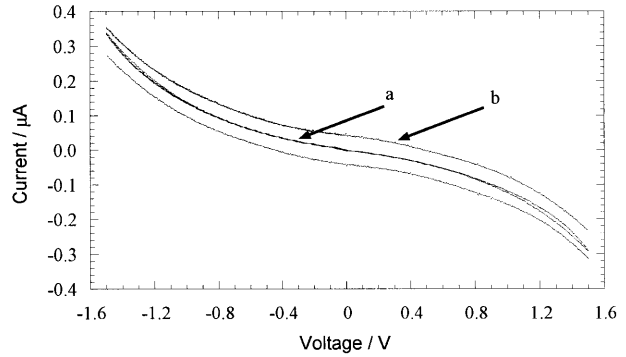

Fig. 2. Current–voltage curves for the Hg–C_{12}–C_{12}–Hg junction formed and recorded in 20% (v/v) solution of dodecanethiol in hexadecane. Scan rates: (a) 0.5 V s^{-1}; (b) 50 V s^{-1}. Junction area $A = 0.0015$ cm^2.

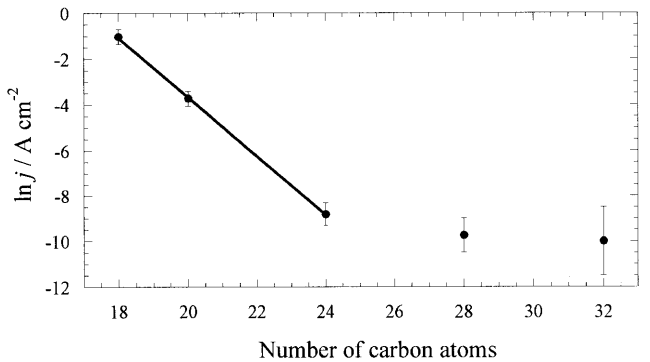

Fig. 3. Plot of the logarithm of the tunneling current density measured at 1.5 V vs. the number of carbon atoms in the alkanethiolate bilayers trapped in the Hg–Hg junctions.

Hg surfaces results in an increase of the junction area. Not surprisingly, these interactions are magnified in water due to the hydrophobic effect. When two alkanethiolate-coated mercury drops are brought into contact at a constant voltage bias, regardless of its magnitude, the junction is formed instantaneously upon the first contact of the two drops. In other words the first step of junction assembly described above is circumvented.

The presence of the van der Waals attraction between the alkanethiolate monolayers and the additional coulombic attraction between Hg surfaces that exists after a voltage bias is applied, both weigh to destabilize the junction with time. This indeed should be expected in view of the known liquid character of the alkanethiolate monolayers on mercury with chain length in the range C_9–C_{16} used in the current investigations. Consequently, a junction with measurable stabilities (with life-time on the order of 100 s or greater) can be formed only with alkanethiols longer than C_8. The stability of the junctions increases with increasing chain length of the alkanethiols. The stability and more specifically the time evolution of the structure of an alkanethiol bilayer in the junction become the focus of the remainder of this report. We are interested in understanding what the magnitude of the structural changes induced by the van der Waals and coulombic forces are and how these changes effect the strength of the electronic coupling across the junction. We point out that single alkanethiolate monolayers on mercury, which we have investigated before, did not show any significant structural changes with time [14].

A typical current–voltage curve recorded for a dodecanethiol junction (Hg–C_{12}–C_{12}–Hg) is shown in Fig. 2. The shape of such current–voltage bias curves depends on the voltage scan rate. For slower scan rates a small hysteresis is observed (see Fig. 2a) reflecting the effect of the applied bias and the time evolution of the bilayer structure in the junction. This effect is larger for thicker junctions. Also, in these cases, an increase of tunneling current (in a region of biases in excess of ca. 1 V) is observed during the second and subsequent cycles suggesting a progressive decrease of the junction thickness. The fact that these effects are more pronounced in the case of thicker junctions (assembled with tetradecane- and hexadecanethiols) can be rationalized by the fact that the longer alkanethiolate monolayers are intrinsically less well ordered. The structure of the alkanethiolate monolayers on mercury has been discussed previously [14,48]. Specifically, we showed that the oxidative coupling of alkanethiols to mercury is a process that proceeds on a millisecond time scale and is arrested when a passivating film of mercuric thiolate forms [14]. Thus formation of longer alkane chain monolayers could result, on this time scale, in somewhat more disordered monolayer films. Under the influence of the van der Waals and coulombic interactions in the junctions, these films appear to be more prone to collapse via a slowly progressing intercalation of the alkane chains.

To measure the electron tunneling decay constant, the logarithm of the tunneling current density measured at a fixed voltage bias (1.5 V) was plotted versus the number of carbon atoms in the bilayer, as shown in Fig. 3. The slope of the plot gives a tunneling constant, $\beta = 1.29$ per CH_2 group (1.0 $Å^{-1}$) when data corresponding only to the C_9–C_9, C_{10}–C_{10}, C_{12}–C_{12} junctions are included in the regression. For these junctions, fast scan (> 50 V s^{-1}) j–V curves could be recorded reproducibly. Due to the short time nature of these experiments, we are reasonably sure that the initial structure of the alkanethiolate bilayer is not yet perturbed by the slowly progressing structural collapse of the junction. The dependence of β on the voltage bias has been discussed in our previous report [23]. Unfortunately, data for the thicker bilayer junctions (C_{14}–C_{14}, C_{16}–C_{16}) had to be recorded at scan rates below 0.5 V s^{-1}. At higher scan rates, the magnitude of the capacitive current background becomes too large relative to the

tunneling current. The significant positive deviation of the C_{14} and C_{16} entries in Fig. 3 from the linear dependence obeyed by the thinner junctions is probably due to the partial collapse of the thicker junctions. It is also possible that conduction processes other then tunneling contribute to the measured currents for thicker junctions [32,35].

To study further the nature of the bilayer collapse processes, we followed the time dependence of the tunneling current at a constant voltage bias (1.5–2.5 V) for a thin (C_{10}–C_{10}) and a thick (C_{16}–C_{16}) junction. Typical I–t traces are shown in Fig. 4. In the case of the C_{16}–C_{16} junction (Fig. 4a), the tunneling current increases with a progressively higher rate culminating in a junction breakdown after $\sim$10–20 min. Clearly, the increase of the tunneling current must be associated with a progressive decrease of the junction thickness due likely to chain–chain intercalation. If a decay constant $\beta = 1.29$ per CH_2 of Fig. 3 is used to interpret

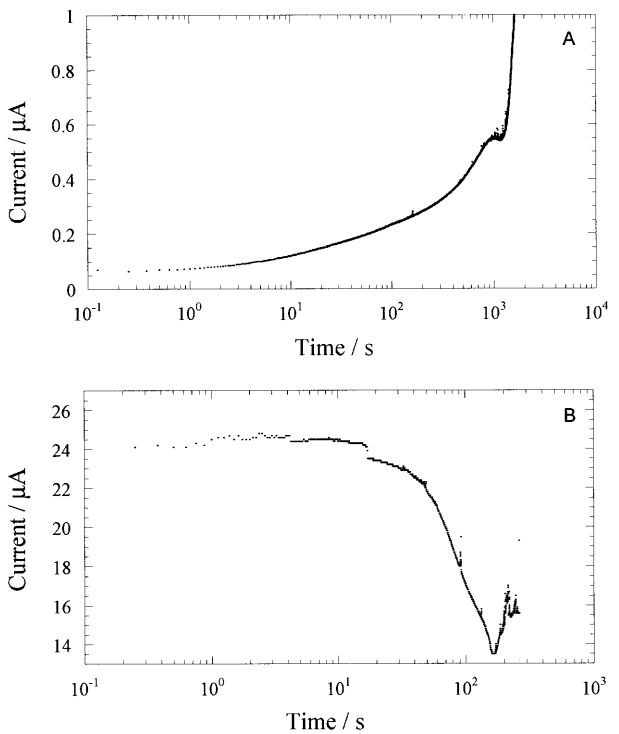

Fig. 4. Current vs. time transients for two alkanethiolate bilayer junctions recorded immediately after their assembly in hexadecane solutions of alkanethiols. (A) C_{16}–C_{16} bilayer, voltage bias $V = 2.5$ V; (B) C_{10}–C_{10} bilayer, $V = 1.5$ V.

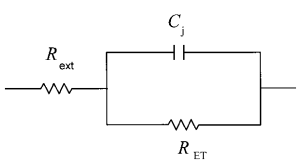

Fig. 5. The equivalent circuit representing Hg–C_n–C_n–Hg tunneling junctions.

the current in Fig. 4a at $t = 1000$ s, the junction thickness decreased by two methylene groups relative to its initial value. A qualitatively different patterns of behavior is observed in the case of thin junctions (see Fig. 4b). While the evolution of the bilayer structure in these junctions is less reproducible, a *decrease of tunneling current* is the most conspicuous and characteristic feature of their I–t curves. Ultimately, this is followed by a current increase and a junction breakdown. Since in order to account for this surprising current decrease one cannot postulate an increase of the junction thickness, the observed decrease must be due to a decrease of the strength of the electronic coupling across the junction. We postulate that this decrease of the electronic coupling strength is due to the formation of *gauche* defects in the initially all-*trans* alkane chains.

3.2. Measurements and interpretation of the junction resistance at zero bias

To test further the hypothesis outlined above, we resorted to impedance spectroscopy in order to decouple the effects of the voltage bias and time as two factors leading to the collapse of these junctions. Specifically, impedance measurements allow us to characterize the kinetics of electron tunneling at zero voltage bias (via tunneling resistance measurements) at a certain time following junction assembly. Furthermore, the impedance measurements allow us to measure junction capacitance simultaneously with the measurements of the tunneling resistance. This is a key advantage allowing us to interpret properly the zero bias junction resistance data. In impedance spectroscopy a sinusoidal voltage signal, $E = E_m \sin(\omega t)$ is applied across a junction and the absolute value of the impedance vector $|\boldsymbol{Z}|$ and the phase angle are measured [49]. Thus both the real and imaginary part of the impedance of the circuit can be determined. As shown in Fig. 5, a tunneling junction can be represented by a parallel combination of a capacitor (C_j) representing the capacitance of the bilayer junction and a resistor (R_{ET}) representing the electron tunneling resistance, coupled in series with another resistor (R_{ext}) due to the resistance of the two Hg capillaries. For this system, the impedance is expressed by the following equations [49]:

$$\boldsymbol{Z}(\omega) = \mathrm{Re}\,\boldsymbol{Z} - \mathrm{Im}\,\boldsymbol{Z} \tag{1}$$

$$\mathrm{Re}\,\boldsymbol{Z} = R_{ext} + \frac{R_{ET}}{1 + (\omega C_j R_{ET})^2} \tag{2}$$

$$\mathrm{Im}\,\boldsymbol{Z} = \mathrm{j}\,\frac{\omega C_j R_{ET}^2}{1 + (\omega C_j R_{ET})^2} \tag{3}$$

The complex–plane impedance plots for the junctions of different thickness are shown on Fig. 6. The C_9–C_9 junctions are not sufficiently stable to be investigated by this technique. This is due to the fact that

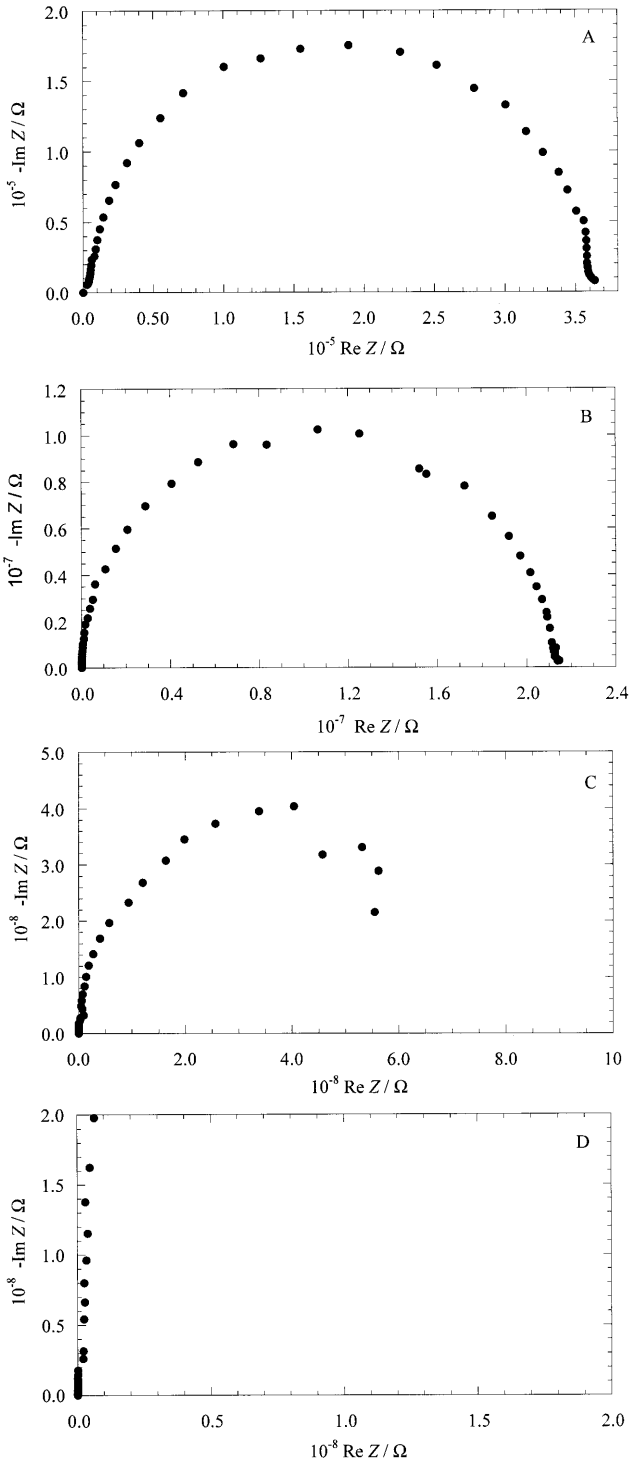

Fig. 6. Complex plane impedance plots for the Hg–C_n–C_n–Hg tunneling junctions under zero voltage bias conditions. The amplitude of the sinusoidal voltage perturbation was $E_m = 25$ mV. (A) C_{10}–C_{10} bilayer, frequency range: 10^4–10^{-2} Hz. (B) C_{12}–C_{12} bilayer, frequency range: 10^4–10^{-2} Hz. (C) C_{14}–C_{14} bilayer, frequency range: 10^4–10^{-2} Hz. (D) C_{16}–C_{16} bilayer, frequency range: 10^4–10^{-2} Hz.

application of the ac voltage perturbation in itself is an addition element destabilizing junctions. We discuss this factor in more details below. While the complex–plane plots for the junctions thinner than C_{16}–C_{16} exhibit, albeit with some deviations, the expected semicircles, the severe distortion in the plot recorded in the latter case indicates clearly that R_{ET} is too high to be measured in the available frequency range of 10^4–10^{-2} Hz. The values of R_{ET} for thinner junctions were obtained by projecting the low frequency values of Re $\boldsymbol{Z}$ to $\omega = 0$ and assuming that the equivalent circuit in Fig. 5 adequately describes the behavior of these junctions. Before we analyze these measurements, it is important to point out, that the R_{ET} values obtained this way probably reflect the properties of the partially collapsed junctions. This is because, due to the nature of the impedance measurements, they were obtained minutes after their assembly. Thus it becomes important to obtain capacitance values for these junctions under exactly the same long time, low frequency conditions in order to deduce then the extent of the junction collapse. We deal with this problem next.

In view of the fact that R_{ET} for the C_{16}–C_{16} junctions is extremely high, the behavior of these junctions can be approximated (within the available frequency range) by an equivalent circuit consisting of C_j and R_{ext} in series for which $\boldsymbol{Z}(\omega)$ is expressed by [49]:

$$\boldsymbol{Z}(\omega) = R_{ext} - j\frac{1}{\omega C_j} \quad (4)$$

Analysis of the data in view of this equation gave the frequency dependence of the C_j shown in Fig. 7. It is conspicuous that in addition to a steady increase of the capacitance with decreasing frequency the junction capacitance also increases stepwise at the points when the instrument changes the range of frequencies. This suggests that the application of the sinusoidal voltage perturbation of variable frequency is an additional factor affecting junction stability. Indeed, when the same junction is exposed to the second cycle of C versus ω experiment identical to that in Fig. 7, the initial capacitance measured at 10^4 Hz is ca. 0.60 μF cm^{-2}. In Fig. 8, we compare the time dependence of a junction capacitance measured at a fixed frequency. The contin-

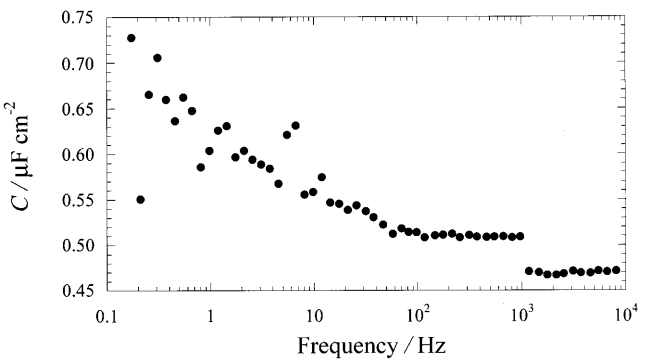

Fig. 7. Plot of capacitance of a Hg–C_{16}–C_{16}–Hg tunneling junction vs. frequency obtained using Eq. (4) and data in Fig. 6(D).

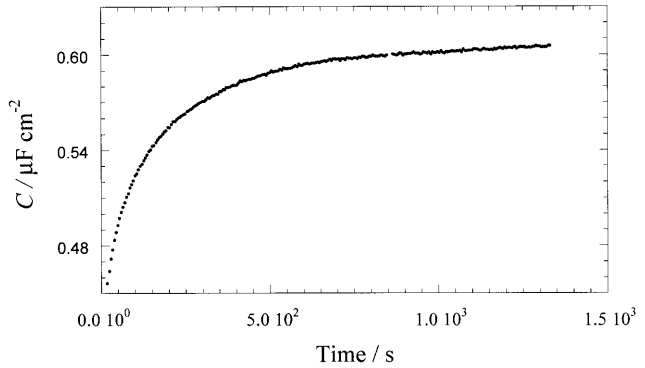

Fig. 8. Dependence of the capacitance of a Hg–C_{16}–C_{16}–Hg tunneling junction vs. time obtained from the impedance measurements at a single frequency $\omega = 10^4$ Hz and evaluated in view of Eq. (4).

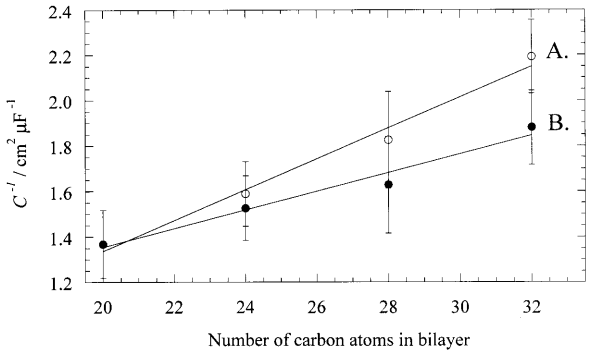

Fig. 9. Plot of the inverse capacitance of the Hg–C_n–C_n–Hg junctions as a function of the number of carbon atoms in the bilayer. (A) The 'short' time, high frequency ($\omega = 10^4$ Hz) capacitance values (C_j short). (B) the 'long' time, low frequency ($\omega = 10$ Hz) capacitance values ($C_{j\ long}$).

uous increase of the capacitance from ca. 0.46 to 0.60 clearly documents the importance and the effect of time on the structure of this junction. However, while the same change of capacitance required only ca. 2 min under the conditions of Fig. 7, it requires ca. 15 min under the constant ω conditions of Fig. 8. Chain–chain intercalation results, in these cases, in a 20% decrease of the junction thickness corresponding to approximately seven methylene groups during the first 200 s. It is interesting to compare this result with an estimate of the extent of chain–chain intercalation in the same junction in a similar experiment of Fig. 4a. In this case, the analysis of the tunneling current increase in the first 1000 s (assuming $\beta = 1.29$ per CH_2 group) suggested only a ca. two methylene group change of the junction thickness. This apparent inconsistency with the result of the capacitance experiment in Fig. 8 is even greater considering the fact that the Fig. 4a experiment was conducted under a 2.5 V bias that generated a substantial coulombic force squeezing the junction in addition to the van der Waals attraction. To reconcile these differences, it is important to appreciate that, in addition to the chain–chain intercalation taking place in both of these experiments, chain disorder (*gauche* defects) is also inevitably induced in the bilayer structure. While the latter does not influence the capacitance data which are sensitive only to the junction thickness, the increase of the tunneling current in Fig. 4a is substantially smaller than expected purely on the basis of the decreased thickness of the junction. A diminished strength of electronic coupling across the bilayer junction due to chain disorder analogous to the case featured in Fig. 4b is an important additional factor, weighing to decrease the tunneling current. In view of this discussion, it is also likely that the structural changes taking place during the experiment of Fig. 4b carried out with a C_{10}–C_{10} junction also involve both generations of the *gauche* defects and chain–chain intercalation. The difference between the C_{10} and C_{16} type junctions lies only in the degree to which these changes take place. A qualitative analysis of the data in Fig. 4a,b suggest that chain–chain intercalation progresses more rapidly in the case of the thicker junction.

Overall, data in Fig. 7 provide us with the short time (high frequency, $\omega = 10^4$ Hz) and the long time (low frequency, $\omega = 10$ Hz) values of the junction capacitance, $C_{j\ short}$ and $C_{j\ long}$, respectively. The 'short' time refers to several seconds after junction assembly while 'long' time corresponds to ca 2.5 min and reflects both the time effects as well as the effects of the variable frequency ac perturbation mentioned above. The same method was used to obtain these values for the C_{14}–C_{14} junctions. In order to obtain $C_{j\ short}$ and $C_{j\ long}$ for the decane and dodecane junctions, the imaginary impedance data of Fig. 6a,b were fit to Eq. (3) over two different ranges of ω. Obtaining the short time C_j values involved the data in the frequency range 10^2–10^4 Hz. The long time C_j values were obtained from the data collected in the range 10–10^2 Hz. While this method is clearly approximate, we find that it offers the two limits of the C_j values with a higher precision than a method based on single frequency data analysis.

The resulting $C_{j\ short}$ and $C_{j\ long}$ values are plotted in Fig. 9 versus the number of the carbon atoms in these junctions. As mentioned above, the $C_{j\ short}$ data represent the initial state of the bilayer structures while the $C_{j\ long}$ plot reflects time dependent structural changes of the alkanethiolate bilayers under the conditions of the impedance measurements. An increasing difference between $C_{j\ short}$ and $C_{j\ long}$ is the key feature of Fig. 9. It reflects a greater tendency of the longer junctions to undergo chain–chain intercalation with time. Assuming a parallel plate capacitor model, the slope of the $C_{j\ short}$ data gave an average dielectric constant $\varepsilon = 2.1$ which is in good agreement with the literature data for ordered alkane monolayers. In these calculations, we assumed all-*trans* conformation of the alkane chains and used 1.255 Å as the projected length of a C–C bond as

described earlier. Since the dielectric properties of the alkanethiolate bilayers should be independent of the extent of their intercalation and disorder, this value of ε was then used to interpret the $C_{j\,long}$ values in terms of the thickness of the partially collapsed junctions. These experimentally determined thickness (d) were used in turn to plot the dependence of ln R_{ET} versus d shown in Fig. 10. Knowing the measured junction areas and the experimental values of the initial surface coverage of alkanethiolate monolayers, the zero voltage bias R_{ET} data were expressed as resistance of a single collinear pair of alkanethiolates. The slope of the plot gives $\beta = 1.6$ Å^{-1} which is substantially higher than $\beta = 1.0$ Å^{-1} obtained from the linear region in Fig. 3. These two values of the decay constant reflect a substantial difference in the electronic coupling strength across alkanethiolate films in largely a well ordered, all-*trans* conformation and in a disordered state.

In conclusion, we have investigated the slowly progressing changes of the structure of alkanethiolate bilayers of different chain length trapped in the Hg–Hg tunneling junctions. Potentiodynamic methods, direct current–time and impedance techniques have been employed to relate the kinetics of electron tunneling to these structural changes. We found that due to the van der Waals and coulombic forces squeezing the junctions, their structure evolves with time. This time evolution also appears to be accelerated by the changing frequency of the sinusoidal voltage of the impedance measurements. The changes involve simultaneous generation of *gauche* defects and chain–chain intercalation and ultimately lead to junction breakdown. Taken collectively, our data suggest strongly that the chain intercalation proceed more rapidly for thicker junctions. The most important finding of this report is the decay constant for the disordered junctions. Its value $\beta = 1.6$ Å^{-1} is substantially higher than $\beta = 1.0$ Å^{-1} obtained for the junctions in largely all-*trans* conformation.

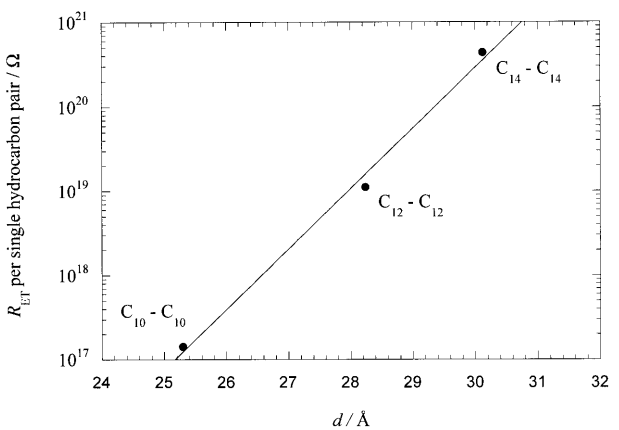

Fig. 10. Plot of electron tunneling resistance calculated per single hydrocarbon pair in a junction as a function of the thickness of the disordered junctions obtained from the $C_{j\,long}$ data in Fig. 9.

While we cannot quantify the extent of chain disorder, our measurements show clearly that such disorder substantially weakens electronic coupling. To this end our measurements disagree with the conclusions of Boulas and co-workers [28] who postulated on the basis of their tunneling junction data that the efficiency of electron tunneling is lowest for the most ordered state of the alkane chains. Our results are in qualitative agreement with the report of Haran and co-workers [27] who also observed a decrease of electrochemically measured tunneling current upon thermally induced chain disorder.

Acknowledgements

Acknowledgement is made to the donors of The Petroleum Research Fund, administered by the ACS, for partial support of this research. Additional support was provided by a grant from the National Science Foundation (CHE-0079225) and by UCB Committee on Research.

References

[1] P.F. Barbara, T.J. Meyer, M.A. Ratner, J. Phys. Chem. 100 (1996) 13248.
[2] C.C. Moser, C.C. Page, R. Farid, P.L. Dutton, J. Bioenerg. Biomembr. 27 (1995) 263.
[3] D.S. Bendall (Ed.), Protein Electron Transfer, BIOS, Oxford, 1996.
[4] W.B. Curry, M.D. Grabe, I.V. Kurnikov, S.S. Skourtis, D.N. Beratan, J.J. Regan, A.J. A. Aquino, P. Beroza, J.N. Onuchic, J. Bioenerg. Biomembr. 27 (1995) 285.
[5] H.B. Gray, J.R. Winkler, Annu. Rev. Biochem. 65 (1996) 537.
[6] H. Grabert, M.H. Devoret, Single Charge Tunneling, Coulomb Blockade Phenomena in Nanostructures, Plenum, New York, 1992.
[7] A. Aviram, M. Ratner, Ann. N.Y. Acad. Sci. 852 (1998) 1.
[8] J. Jortner, M. Ratner, Molecular Electronics, IUPAC, Oxford, 1997.
[9] G.L. Closs, J.R. Miller, Science 240 (1988) 440.
[10] C.E.D. Chidsey, Science 251 (1991) 919.
[11] S.B. Sachs, S.P. Dudek, R.P. Hsung, L.R. Sita, J.F. Smalley, M.D. Newton, S.W. Feldberg, C.E.D. Chidsey, J. Am. Chem. Soc. 119 (1997) 10563.
[12] J. Cheng, G. Saghi-Szabo, J.A. Tossell, C.J. Miller, J. Am. Chem. Soc. 118 (1996) 680.
[13] M.R. Arkin, E.D.A. Stemp, R.E. Holmlin, J.K. Barton, A. Hormann, E.J.C. Olson, P.F. Barbara, Science 273 (1996) 475.
[14] K. Slowinski, R.V. Chamberlain, C.J. Miller, M. Majda, J. Am. Chem. Soc. 119 (1997) 11910.
[15] S.S. Isied, I. Moreira, M.Y. Ogawa, A. Vassilian, B. Arbo, J. Sun, J. Photochem. Photobiol. A: Chem. 82 (1994) 203.
[16] R.A. Marcus, N. Sutin, Biochim. Biophys. Acta 811 (1985) 265.
[17] C. Miller, P. Cuendet, M. Gratzel, J. Phys. Chem. 95 (1991) 877.
[18] J.F. Smalley, S.W. Feldberg, C.E.D. Chidsey, M.R. Linford, M.D. Newton, Y.-P. Liu, J. Phys. Chem. 99 (1995) 13141.
[19] H.O. Finklea, D.D. Hanshew, J. Am. Chem. Soc. 114 (1992) 3173.
[20] W.B. Davis, M.A. Ratner, M.R. Wasielewski, Nature 396 (1998) 60.

[21] S. Creager, C.J. Yu, C. Bamdad, S. O'Connor, T. MacLean, E. Lam, C.Y.G.T. Olsen, J. Luo, M. Gozin, J.F. Kayyem, J. Am. Chem. Soc. 121 (1999) 1059.
[22] R.S. Clegg, J.E. Hutchison, Meeting Abstracts, vol. 99–1, The Electrochemical Society, 1999.
[23] K. Slowinski, H.K.Y. Fong, M. Majda, J. Am. Chem. Soc. 121 (1999) 7257.
[24] D.N. Beratan, J.N. Onuchic, J.R. Winkler, H.B. Gray, Science 258 (1992) 1740.
[25] M.D. Newton, Chem. Rev. 91 (1991) 767.
[26] K.D. Jordan, M.N. Paddon-Row, Chem. Rev. 92 (1992) 395.
[27] A. Haran, D.H. Waldeck, R. Naaman, E. Moons, D. Cahen, Science 263 (1994) 948.
[28] C. Boulas, J.V. Davidovits, F. Rondelez, D. Vouillaume, Phys. Rev. Lett. 76 (1996) 4797.
[29] H.O. Finklea, in: A.J. Bard, I. Rubinstein (Eds.), Electroanalytical Chemistry, vol. 19, Marcel Dekker, New York, 1996, p. 109.
[30] A. Ulman, An Introduction to Ultrathin Organic Films: From Langmuir–Blodgett to Self-Assembly, Academic Press, San Diego, CA, 1991, p. 367 (Chapter 5.4).
[31] M.C. Petty, Langmuir–Blodgett Films, Cambridge University Press, Cambridge, 1996, p. 131 (Chapter 6).
[32] B. Mann, H. Kuhn, J. Appl. Phys. 42 (1971) 4398.
[33] E.E. Polymeropoulos, J. Sagiv, J. Chem. Phys. 69 (1978) 1836.
[34] R.H. Tredgold, A.J. Vickers, R.A. Allen, J. Phys. D: Appl. Phys. 17 (1984) L5.
[35] N.J. Geddes, J.R. Sambies, W.G. Parker, N.R. Couch, D.J. Jarvist, J. Phys. D: Appl. Phys. 23 (1990) 95.
[36] A. Barraud, P. Millie, I. Yakimenko, J. Chem. Phys. 105 (1996) 6972.
[37] C. Zhou, M.R. Deshpande, M.A. Reed, L. Joness 11, J.M. Tour, Appl. Phys. Lett. 71 (1997) 611.
[38] M.A. Reed, C. Zhou, C.J. Muller, T.P. Burgin, J.M. Tour, Science 278 (1997) 252.
[39] S.J. Tans, A.R.M. Verschueren, C. Dekkar, Nature 393 (1998) 49.
[40] C.P. Collier, E.W. Wong, M. Belohradsky, F.M. Raymo, J.F. Stoddard, P.J. Kuekes, R.S. Williams, J.R. Heath, Science 285 (1999) 391.
[41] G. Leatherman, E.N. Durantini, D. Gust, T.A. Moore, A.L. Moore, S. Stone, Z. Zhou, P. Rez, Y.Z. Liu, S.M. Lindsay, J. Phys. Chem. B 103 (1999) 4006.
[42] D.J. Wold, C.D. Frisbie, J. Am. Chem. Soc. (2000) in press.
[43] L.A. Bumm, J.J. Arnold, T.D. Dunbar, D.L. Allara, P.S. Weiss, J. Phys. Chem. B (1999) 8122.
[44] J.D. Porter, A.S. Zinn, J. Phys. Chem. 97 (1993) 1190.
[45] S. Usui, T. Yamasaki, J. Shimoizaka, J. Phys. Chem. 71 (1967) 3195.
[46] M.A. Rampi, O.J.A. Schueller, G.M. Whitesides, Appl. Phys. Lett. 72 (1998) 1781.
[47] W. Kemula, Z. Kublik, Anal. Chim. Acta 18 (1958) 104.
[48] O.M. Magnussen, B.M. Ocko, M. Deutsch, M.J. Regan, P.S. Pershan, D. Abernathy, G. Gruebel, J.-F. Legrand, Nature 384 (1996) 250.
[49] E. Gileadi, Electrode Kinetics for Chemists, Chemical Engineers, and Material Scientists, VCH, New York, 1993, pp. 213, 428 (Chapters 16 and 26.